

Technical Foundations: Late Gadolinium Enhancement Imaging Techniques

Peter Kellman, NIH/NHLBI

Background

Late gadolinium enhancement (LGE), often referred to as simply late enhancement imaging or delayed enhancement, has become a gold standard in myocardial viability assessment (1,2). Late enhancement imaging provides excellent depiction of myocardial infarction (MI) and macroscopic scarring. The use of late enhancement in the diagnosis of ischemic heart disease and in guiding therapy such as revascularization has gained wide acceptance. More recently, late enhancement is playing a broader role in characterizing fibrosis in non-ischemic cardiomyopathies (3,4), and in measurement of scar resulting from treatment such as electrophysiology guided ablation (5).

Late enhancement imaging is used to diagnose and characterize a wide range of ischemic and non-ischemic cardiomyopathies, and its use has become ubiquitous in the cardiac MR exam. As the use of late enhancement imaging has matured and the span of applications has widened, the demands on image quality have grown (6). To gain a better understanding of the imaging requirements and technical challenges, it is worthwhile to examine the range of applications and variety of late enhancement patterns (Fig. 1). As imaging techniques have improved, the characterization of sub-endocardial MI now includes the accurate quantification of scar size, shape, and characterization of borders which have been shown to have prognostic significance (7–11). More diverse patterns of late enhancement including patchy, mid-wall, sub-epicardial, or diffuse enhancement are of interest in diagnosing non-ischemic cardiomyopathies such as ARVD, HCM, DCM, myocarditis, sarcoidosis, amyloidosis, and muscular dystrophy (4,12–17). As clinicians are examining late enhancement images for more subtle indication of fibrosis, the demand for lower artifacts has increased.

A range of new techniques have emerged to improve the speed and quality of late enhancement imaging. These include single shot imaging and motion corrected averaging for acquisition during free breathing, and fat water separated imaging for characterizing fibro-fatty infiltration and reduction of artifacts related to the presence of fat. Using conventional late enhancement methods it is difficult to discriminate globally diffuse fibrosis from normal healthy tissue. Methods for quantification of T1 and extracellular volume fraction are emerging to tackle this issue.

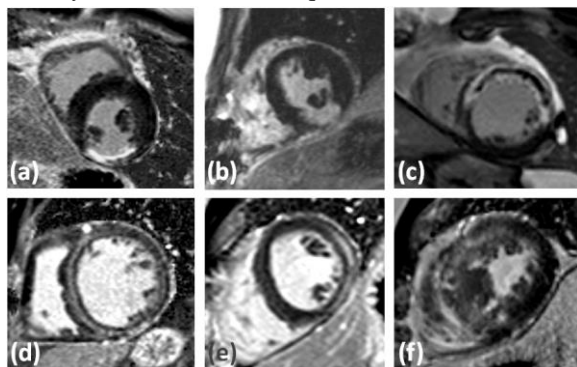


Figure 1. Examples late enhancement images illustrating the a variety of late enhancement patterns (a) sub-endocardial chronic MI, (b) transmural chronic MI, (c) acute MI with dark core due to microvascular obstruction, (d) mid-wall enhancement in patient with myocarditis, (e) sub-epicardial enhancement in patient with myocarditis, (f) patchy appearance of scarring in a patient with HCM.

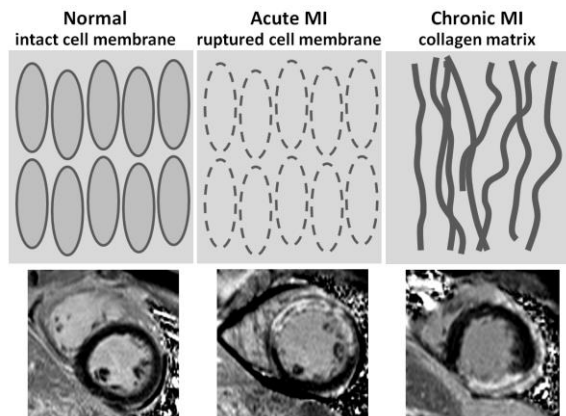
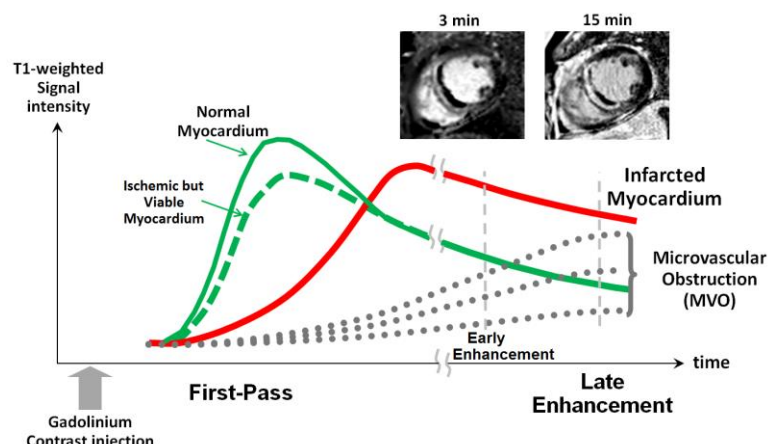
Basis for late contrast enhancement

Contrast enhancement using gadolinium (Gd) agents is based on T1-shortening and the distribution of contrast agent within the tissue. The mechanism of early and late enhancement relates to the different wash-in and wash-out kinetics of normal myocardium and tissue with myocardial infarction or fibrosis (18,19). Following administration of a bolus of gadolinium contrast agent, the contrast will reach the various tissue compartments within the myocardium at different rates until a dynamic steady state is reached (Fig. 2). The commonly used Gd based contrast agents with large molecular weight are extracellular and will generally take a longer time to wash-in and-out of the infarcted tissue than normal healthy cells. Gadolinium will take even longer to reach regions that have microvascular obstruction (MVO).

The extracellular volume fraction (ECV) in regions of infarcted myocardium (Fig. 3) is significantly higher than that of regions with normal healthy cells and thus have a higher concentration of gadolinium. In the case of acute MI with rupture of the cell membrane, the gadolinium enters the extracellular space and what had previously been intracellular space. For chronic MI with cell replacement by a matrix of collagen the extracellular space is substantially increased. There is a linear relationship between the relaxivity of longitudinal magnetization ($R_1 =$

$1/T1$) and the change in contrast agent concentration, $\Delta R1 = R1_{\text{post}} - R1_{\text{pre}} = \gamma [Gd]$. Regions with a greater extracellular volume fraction (ECV) will have a higher concentration of contrast agent ($[Gd]$) at steady state and will experience greater $T1$ -shortening. These regions will appear brighter on $T1$ -weighted images, for example using inversion recovery.

Figure 2. Signal intensity time course from administration of bolus through late enhancement illustrating slower wash-in and wash-out of Gd contrast into infarcted tissue compared with normal ischemic tissue. Tissue with microvascular obstruction (MVO) experiences very slow wash-in of Gd. The apparent size of MVO region in acute MI shrinks between early (3 min) and late (15 min) enhancement images due to late arrival of Gd.



intensity of infarcted tissue is bright on the $T1$ -weighted image, typically brighter than both the blood pool and normal myocardium (Fig. 3). The relative contrast between the MI, blood pool, and normal myocardium depends on a number of factors such as contrast agent dose, time from dose, and clearance rate.

Inversion recovery images are typically acquired in mid to late diastole in order to minimize cardiac motion. The inversion recovery time is typically chosen to null the normal myocardium which provides the best tissue contrast between MI and normal myocardium in the case of magnitude image reconstruction (Fig 4). Normal myocardium will appear black, and the MI with higher gadolinium concentration and consequently shorter $T1$ and faster recovery will appear bright. The gadolinium concentration in the blood is often at an intermediate concentration dependent on a number of factors, and thus would have intermediate signal intensity. The TI to null the normal myocardium may be determined either by multiple acquisitions on a trial and error basis or by means of a cine-IR-SSFP scout (21) which acquires a number of TI's in a segmented fashion, each at different cardiac phases. In the latter case using an IR cine TI scout, the null time may be underestimated since inversion recovery is influenced by the readout causing a shorter apparent $T1$ referred to as $T1^*$ (22) which depends on specific protocol parameters. Alternatively, a direct $T1$ mapping measurement may be made using a modified Look Locker inversion recovery (MOLLI) method (23) to determine appropriate TI to null the normal myocardium.

In cases for which the TI is set shorter than the time to null the normal myocardium the loss of polarity in the magnitude reconstructed image will result in a loss of contrast. The positive signal may also appear as an artifact. PSIR reconstruction preserves polarity and is therefore much less sensitive to the inversion time (Fig. 5) (6,24,25). For PSIR late enhancement the polarity is restored, and may be retrospectively window and leveled to display the normal myocardium as black while the MI will appear bright.

Figure 3. Illustration of extracellular volume fraction for normal myocardium with intact cell membrane, acute MI with ruptured cell membrane, and chronic MI with collagen matrix.

Late Enhancement Imaging

LGE may be imaged using an inversion recovery (IR) sequence to provide $T1$ -weighting with good contrast-to-noise (20). Infarcted myocardium or fibrotic scar tissue exhibits late enhancement typically 10-20 min following administration of Gd-DTPA (0.1-0.2 mmol/kg). The signal

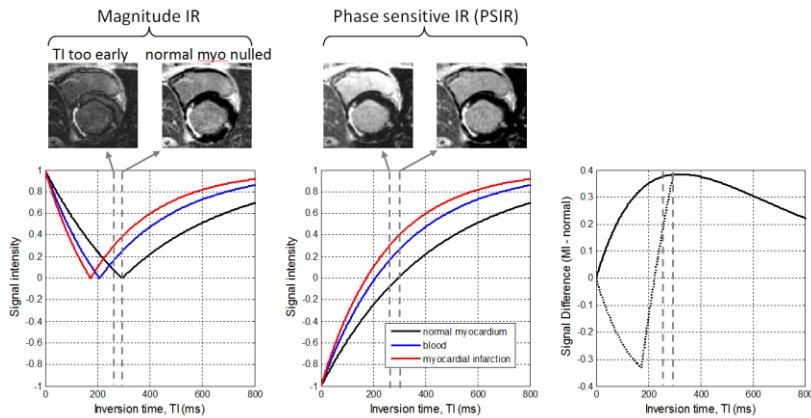


Figure 4. Signal intensity versus inversion time is plotted for magnitude inversion recovery (MagIR) (left) and phase sensitive inversion recovery (PSIR) (center), and signal difference between MI and normal myocardium (right) illustrates the sensitivity of MagIR to setting the inversion time (TI) to null the normal myocardium. MagIR exhibits a loss of contrast (dotted line) and polarity artifact when the TI is too early, whereas PSIR (solid line) maintains a similar appearance.

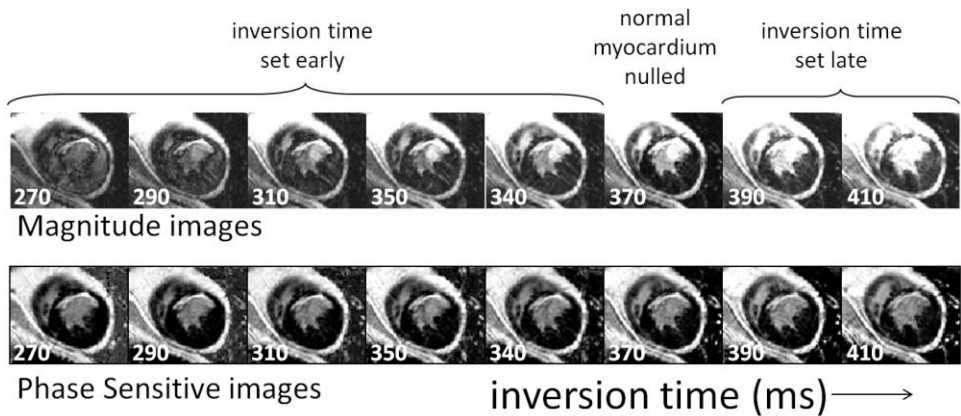
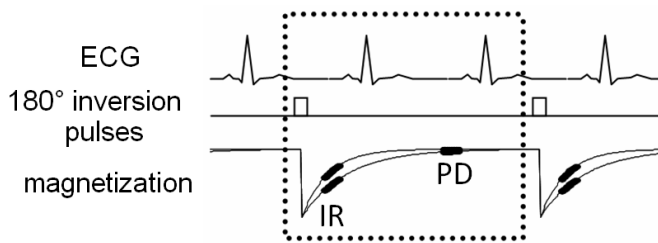


Figure 5. Magnitude IR (top) and PSIR (bottom) reconstructed late enhancement images acquired at a series of TIs illustrating the relative TI insensitivity of PSIR over a wide range.

PSIR sequences typically acquire both an IR and a proton density (PD) weighted image at the same cardiac and respiratory phase to provide a reference for background phase, and for correcting surface coil intensity variation (26). With inversions every 2 R-R's the PD image may be acquired on alternate heartbeats (Fig 6) after the magnetization has substantially recovered and is essentially positive. A lower excitation flip angle for readout of the PD image is used in order not to steal too much of the magnetization, and to better approximate a PD weighting.

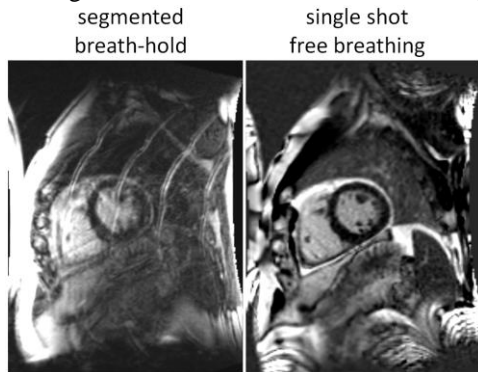
Figure 6. Timing of inversion recovery for segmented PSIR with inversions every 2 R-R intervals including acquisition of PD-weighted reference data on alternate heartbeats.



A number of variations of IR imaging sequences are possible, each with their pros and cons. LGE imaging may be performed using a breath-held conventional segmented acquisition, or free-breathing using either navigators or single-shot imaging (27,28). Imaging may be 2D-multislice or 3D. Readouts may use either FLASH or SSFP. Acquisitions may be accelerated by means of parallel imaging. For each slice, imaging is performed in mid-diastole following non-selective 180° inversion using an adiabatic pulse applied every other heartbeat to permit nearly full recovery of magnetization in the presence of Gd-DTPA (Fig. 6). Prospectively gated k -space data is acquired at TI following the inversion. Using inversion every RR decreases the acquisition time but increases sensitivity to RR variation which may lead to artifacts.

Acquisition may be segmented or single-shot. For segmented FLASH acquisition, typical sequence parameters are (29): 25° readout flip angle, 16-25 views per segment, 256x128 matrix, acquired in approx. 12-16 heartbeats (with inversions every 2RR), TR=8.4ms, BW=140 Hz/pixel. Typical spatial resolution is 1.4x2.1 mm² for 360x270 mm²

rectangular FOV. Single-shot, PSIR-SSFP may be used for rapid acquisition to acquire multiple 2D slices covering the entire heart in a single breath-hold (30), or may be used in cases of arrhythmias or difficulty breath-holding when segmented breath-hold scans may result in ghost artifacts (Fig. 7) (6,28,30–32). For single-shot SSFP acquisition, typical sequence parameters are: 50° readout flip angle, 192x90 matrix, acquired in a single heartbeat (2 heartbeats for PSIR), TR=2.7ms, BW=1000 Hz/pixel. Parallel imaging may be used to decrease the acquisition time for segmented scans, or to reduce the imaging window allowing increased matrix size (256x144) in single-shot



free breathing protocol (right).

imaging. The SNR of single shot PSIR-SSFP may be significantly improved by averaging multiple repeated measurements (Fig. 8). Motion corrected averaging may be used to correct respiratory motion (6,31,32) in the case of free-breathing acquisition, or diaphragmatic drift in the case of breath-holding. Typically, using 8 frames acquired in 16 heartbeats provides an SNR comparable or better than the FLASH protocol for approximately the same duration and may be extended to a larger number of averages since the acquisition is not breath-held.

Figure 7. Illustration of respiratory ghost artifacts (left) segmented breath-held late enhancement imaging in situation where patient has difficulty holding their breath which is mitigated using a single-shot

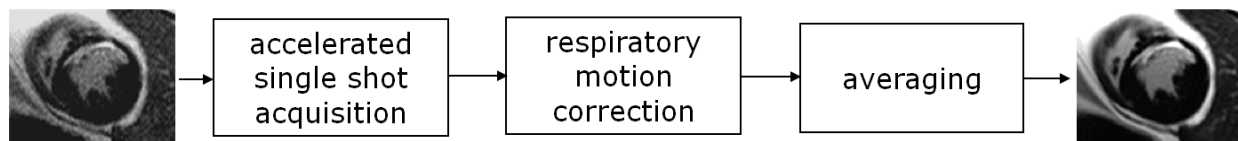


Figure 8. Respiratory motion corrected averaging of multiple accelerated single shot PSIR-SSFP images acquired during free-breathing may be used to improve the SNR becoming comparable or better than breath-held PSIR FLASH protocols for the same duration acquisition.

Acute MI will frequently have regions of microvascular obstruction (MVO) which appear as a dark core or no-reflow zone (Fig 9.) MVO in acute MI has been shown to have prognostic significance (33). MVO may be detected with greater sensitivity early rather than late as shown in Fig. 10.



Fig. 10.

Figure 9. Acute MI with microvascular obstruction (MVO) leads to dark core also known as no-reflow zone within bright MI region.

Figure 10. Early enhancement of acute MI with MVO illustrating the changing size and appearance of MVO with time following contrast administration, acquired at 1 minute intervals starting at 1 min (left) thru 7 min (right) using single shot IR-SSFP-PSIR.

The presence of fibro-fatty infiltration or other intramyocardial fat may have diagnostic value. Using conventional late enhancement imaging, it is difficult to discriminate between fibrosis and intramyocardial fat since both have low T1 and appear bright. Furthermore, the presence of fat may create image artifacts due to the chemical shift of fat or the bright epicardial fat signal may obscure the sub-epicardium. Using fat-water separated late-enhancement imaging it is possible to distinguish the fibrosis from fat (6,34–36) with improved sensitivity and to avoid erroneous tissue classification. Detection and characterization of fat versus fibro-fatty infiltration has potential significance in patients with ARVD (37) or in cases of fatty replacement in chronic MI (35,36). Multi-echo Dixon methods for fat-

water separated late enhancement (34,35) may be used to image fibro-fatty infiltration and discriminate erroneous classification of fat as scar tissue. A case of fatty replacement in patient with chronic MI is shown in Fig. 11.

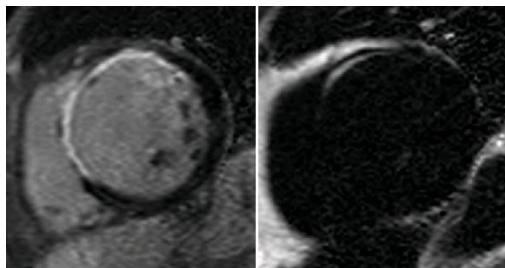


Fig. 11. Multi-echo IR-GRE fat water separated late enhancement for patient with chronic MI with fatty replacement (water is left and fat is right).

Conclusion

Late gadolinium enhancement imaging is widely used and has become a standard for assessment of viability and general characterization of a broad range of both non-ischemic and ischemic cardiomyopathies. As the number of applications has grown and encompass more subtle characteristics such as size and shape of the infarct border zone, or early detection of fibrosis, so have the demands for improved image quality. Methods for mitigating artifacts due to motion and/or arrhythmias have been developed which further increase the robustness of late enhancement imaging. The detection of fibro-fatty infiltration or other intramyocardial fat is possible by means of fat-water separated late enhancement, which also serves to mitigate a number of artifacts that may arise due to the presence of fat.

1. Kim RJ, Fieno DS, Parrish TB, Harris K, Chen E-L, Simonetti O, Bundy J, Finn JP, Klocke FJ, Judd RM. Relationship of MRI Delayed Contrast Enhancement to Irreversible Injury, Infarct Age, and Contractile Function. *Circulation* [Internet] 1999;100:1992–2002. doi: 10.1161/01.CIR.100.19.1992.
2. Kim R, Wu E, Rafael A, Chen E, Parker M, Simonetti O, Klocke F, Bonow R, Judd R. The use of contrast-enhanced magnetic resonance imaging to identify reversible myocardial dysfunction. *N. Engl. J. Med.* 2000;343:1445–1453.
3. Bohl S, Wassmuth R, Abdel-Aty H, Rudolph A, Messroghli D, Dietz R, Schulz-Menger J. Delayed enhancement cardiac magnetic resonance imaging reveals typical patterns of myocardial injury in patients with various forms of non-ischemic heart disease. *Int. J. Cardiovasc. Imaging* [Internet] 2008;24:597–607. doi: 10.1007/s10554-008-9300-x.
4. Hunold P, Schlosser T, Vogt FM, Eggebrecht H, Schermund A, Bruder O, Schüler WO, Barkhausen J. Myocardial Late Enhancement in Contrast-Enhanced Cardiac MRI : and Non – Infarction-Related Disease. *AJR. Am. J. Roentgenol.* 2005;184:1420–1426.
5. Vergara GR, Marrouche NF. Tailored management of atrial fibrillation using a LGE-MRI based model: from the clinic to the electrophysiology laboratory. *J. Cardiovasc. Electrophysiol.* [Internet] 2011;22:481–7. doi: 10.1111/j.1540-8167.2010.01941.x.
6. Kellman P, Arai AE. Cardiac imaging techniques for physicians: Late enhancement. *J. Magn. Reson. Imaging* [Internet] 2012;36:529–42. doi: 10.1002/jmri.23605.
7. Amado LC, Gerber BL, Gupta SN, Rettmann DW, Szarf G, Schock R, Nasir K, Kraitchman DL, Lima J a C. Accurate and objective infarct sizing by contrast-enhanced magnetic resonance imaging in a canine myocardial infarction model. *J. Am. Coll. Cardiol.* [Internet] 2004;44:2383–9. doi: 10.1016/j.jacc.2004.09.020.
8. Hsu L-Y, Ingkanisorn WP, Kellman P, Aletras AH, Arai AE. Quantitative myocardial infarction on delayed enhancement MRI. Part II: Clinical application of an automated feature analysis and combined thresholding infarct sizing algorithm. *J. Magn. Reson. Imaging* [Internet] 2006;23:309–14. doi: 10.1002/jmri.20495.
9. Hsu L, Natanzon A, Kellman P, Hirsch GA, Aletras AH, Arai AE. Quantitative Myocardial Infarction on Delayed Enhancement MRI . Part I : Animal Validation of an Automated Feature Analysis and Combined Thresholding Infarct Sizing Algorithm. *J. Magn. Reson. Imaging* 2006;23:298–308. doi: 10.1002/jmri.20496.
10. Fernandez V, Wu KC, Rosen BD, Tomaselli G, Marba E. Enhanced Infarct Border Zone Inducibility of Monomorphic Ventricular Tachycardia in Patients with Ischemic Cardiomyopathy. *Radiology* 2007;245:712–719.
11. Yan AT, Shayne AJ, Brown K a, Gupta SN, Chan CW, Luu TM, Di Carli MF, Reynolds HG, Stevenson WG, Kwong RY. Characterization of the peri-infarct zone by contrast-enhanced cardiac magnetic resonance imaging is a powerful predictor of post-myocardial infarction mortality. *Circulation* [Internet] 2006;114:32–9. doi: 10.1161/CIRCULATIONAHA.106.613414.
12. Puchalski MD, Williams R V, Askovich B, Sower CT, Hor KH, Su JT, Pack N, Dibella E, Gottliebson WM. Late gadolinium enhancement: precursor to cardiomyopathy in Duchenne muscular dystrophy? *Int. J. Cardiovasc. Imaging* [Internet] 2009;25:57–63. doi: 10.1007/s10554-008-9352-y.
13. Moon JC., McKenna WJ, McCrohon J a, Elliott PM, Smith GC, Pennell DJ. Toward clinical risk assessment in hypertrophic cardiomyopathy with gadolinium cardiovascular magnetic resonance. *J. Am. Coll. Cardiol.* [Internet] 2003;41:1561–1567. doi: 10.1016/S0735-1097(03)00189-X.
14. Maceira AM, Joshi J, Prasad SK, Moon JC, Perugini E, Harding I, Sheppard MN, Poole-Wilson PA, Hawkins PN, Pennell DJ. Cardiovascular magnetic resonance in cardiac amyloidosis. *Circulation* [Internet] 2005;111:186–93. doi: 10.1161/01.CIR.0000152819.97857.9D.

15. Bluemke D a., Krupinski EA, Ovitt T, et al. MR Imaging of Arrhythmogenic Right Ventricular Cardiomyopathy: Morphologic Findings and Interobserver Reliability. *Cardiology* [Internet] 2003;99:153–162. doi: 10.1159/000070672.
16. McCrohon J, Moon JCC, Prasad SK, McKenna WJ, Lorenz CH, Coats AS, Pennell DJ. Differentiation of heart failure related to dilated cardiomyopathy and coronary artery disease using gadolinium-enhanced cardiovascular magnetic resonance. *Circulation* [Internet] 2003;108:54–9. doi: 10.1161/01.CIR.0000078641.19365.4C.
17. Sen-Chowdhry S, Syrris P, Prasad SK, Hughes SE, Merrifield R, Ward D, Pennell DJ, McKenna WJ. Left-dominant arrhythmogenic cardiomyopathy: an under-recognized clinical entity. *J. Am. Coll. Cardiol.* [Internet] 2008;52:2175–87. doi: 10.1016/j.jacc.2008.09.019.
18. Arheden H, Saeed M, Higgins CB, Gao D, Bremerich J, Wyttenbach R, Dae MW, Wendland MF. Measurement of the Gadopentetate Dimegлюmine at Echo-planar MR Imaging to Quantify Myocardial Infarction: Comparison with 99m Tc-DTPA Autoradiography in Rats. *Radiology* 1999;311:698–708.
19. Mahrholdt H, Wagner a, Judd RM, Sechtem U. Assessment of myocardial viability by cardiovascular magnetic resonance imaging. *Eur. Heart J.* [Internet] 2002;23:602–19. doi: 10.1053/euhj.2001.3038.
20. Simonetti OP, Kim RJ, Fieno DS, Hillenbrand HB, Wu E, Bundy JM, Finn JP, Judd RM. Cardiac Imaging Technique for the Visualization of Myocardial Infarction. *Radiology* 2001;218:215–223.
21. Gupta A, Lee VS, Chung Y, Babb JS, Simonetti OP. Myocardial Infarction: Optimization of Inversion Times at Delayed Contrast-enhanced MR Imaging. *Radiology* 2004;233:921–926.
22. Schmitt P, Griswold M a, Jakob PM, Kotas M, Gulani V, Flentje M, Haase A. Inversion recovery TrueFISP: quantification of T(1), T(2), and spin density. *Magn. Reson. Med.* [Internet] 2004;51:661–7. doi: 10.1002/mrm.20058.
23. Messroghli DR, Greiser A, Fröhlich M, Dietz R, Schulz-Menger J. Optimization and validation of a fully-integrated pulse sequence for modified look-locker inversion-recovery (MOLLI) T1 mapping of the heart. *J. Magn. Reson. Imaging* [Internet] 2007;26:1081–6. doi: 10.1002/jmri.21199.
24. Huber A, Schoenberg SO, Spannagl B, Rieber J, Erhard I, Klauss V, Reiser MF. Single-shot inversion recovery TrueFISP for assessment of myocardial infarction. *AJR. Am. J. Roentgenol.* [Internet] 2006;186:627–33. doi: 10.2214/AJR.04.0746.
25. Setser RM, Chung YC, Weaver J a, Stillman AE, Simonetti OP, White RD. Effect of inversion time on delayed-enhancement magnetic resonance imaging with and without phase-sensitive reconstruction. *J. Magn. Reson. Imaging* [Internet] 2005;21:650–5. doi: 10.1002/jmri.20323.
26. Kellman P, Arai AE, McVeigh ER, Aletras AH. Phase-Sensitive Inversion Recovery for Detecting Myocardial Infarction Using Gadolinium-Delayed Hyperenhancement. *Magn. Reson. Med.* 2002;38:372–383. doi: 10.1002/mrm.10051.
27. Huber AM, Schoenberg SO, Hayes C, Spannagl B, Engelmann MG, Franz WM, Reiser MF. Phase-Sensitive Inversion-Recovery MR Imaging in the Detection of Myocardial Infarction. *Radiology* 2005;237:854–860.
28. Sievers B, Elliott MD, Hurwitz LM, Albert TSE, Klem I, Rehwald WG, Parker M a, Judd RM, Kim RJ. Rapid detection of myocardial infarction by subsecond, free-breathing delayed contrast-enhancement cardiovascular magnetic resonance. *Circulation* [Internet] 2007;115:236–44. doi: 10.1161/CIRCULATIONAHA.106.635409.
29. Kim RJ, Shah DJ, Judd RM. How We Perform Delayed Enhancement Imaging. *J. Cardiovasc. Magn. Reson.* [Internet] 2003;5:505–514. doi: 10.1081/JCMR-120022267.
30. Huber A, Hayes C, Spannagl B, Rieber J, Klauss V, Schoenberg SO, Reiser M, Wintersperger BJ. Phase-sensitive inversion recovery single-shot balanced steady-state free precession for detection of myocardial infarction during a single breathhold. *Acad. Radiol.* [Internet] 2007;14:1500–8. doi: 10.1016/j.acra.2007.06.017.
31. Kellman P, Larson AC, Hsu L-Y, Chung Y-C, Simonetti OP, McVeigh ER, Arai AE. Motion-corrected free-breathing delayed enhancement imaging of myocardial infarction. *Magn. Reson. Med.* [Internet] 2005;53:194–200. doi: 10.1002/mrm.20333.
32. Ledesma-Carbayo MJ, Kellman P, Hsu L-Y, Arai AE, McVeigh ER. Motion corrected free-breathing delayed-enhancement imaging of myocardial infarction using nonrigid registration. *J. Magn. Reson. Imaging* [Internet] 2007;26:184–90. doi: 10.1002/jmri.20957.
33. Wu KC, Zerhouni E a., Judd RM, Lugo-Olivieri CH, Barouch L a., Schulman SP, Blumenthal RS, Lima J a. C. Prognostic Significance of Microvascular Obstruction by Magnetic Resonance Imaging in Patients With Acute Myocardial Infarction. *Circulation* [Internet] 1998;97:765–772. doi: 10.1161/01.CIR.97.8.765.
34. Kellman P, Hernando D, Arai AE. Myocardial Fat Imaging. *Curr. Cardiovasc. Imaging Rep.* [Internet] 2010;3:83–91. doi: 10.1007/s12410-010-9012-1.
35. Kellman P, Hernando D, Shah S, Zuehlsdorff S, Jerecic R, Mancini C, Liang Z-P, Arai AE. Multiecho dixon fat and water separation method for detecting fibrofatty infiltration in the myocardium. *Magn. Reson. Med.* [Internet] 2009;61:215–21. doi: 10.1002/mrm.21657.
36. Goldfarb JW. Fat-water separated delayed hyperenhanced myocardial infarct imaging. *Magn. Reson. Med.* [Internet] 2008;60:503–9. doi: 10.1002/mrm.21685.
37. Burke A, Farb A, Tashko G, Virmani R. Arrhythmogenic Right Ventricular Cardiomyopathy and Fatty Replacement of the Right Ventricular Myocardium: Are They Different Diseases? *Circulation* [Internet] 1998;97:1571–1580. doi: 10.1161/01.CIR.97.16.1571.